Constraining the composition and thermal state of the mantle beneath Europe from inversion of long-period electromagnetic sounding data

A. Khan,[1] J. A. D. Connolly,[2] and N. Olsen[3]

Received 9 January 2006; revised 23 March 2006; accepted 29 March 2006; published 12 October 2006.

[1] We reexamine the problem of inverting *C* responses, covering periods between 1 month and 1 year collected from 42 European observatories, to constrain the internal structure of the Earth. Earlier studies used the *C* responses, which connect the magnetic vertical component and the horizontal gradient of the horizontal components of electromagnetic variations, to obtain the conductivity profile of the Earth's mantle. Here, we go beyond this approach by inverting directly for chemical composition and thermal state of the Earth, rather than subsurface electrical conductivity structure. The primary inversion parameters are the composition of the Earth's mantle within the system CaO-FeO-MgO-Al_2O_3-SiO_2 and geotherm. Given these parameters, we calculate mineral modes at the prevailing physical conditions and combine these with laboratory-based models for the conductivity of individual minerals to estimate the bulk Earth electrical conductivity structure from which *C* responses are calculated. To further constrain the radial density profile, we also invert for mass and moment of inertia. The results agree with earlier geophysically derived conductivity and seismic velocity models and confirm that inversion of geophysical data for compositional parameters, planetary composition, and thermal state is feasible. The inversion indicates most probable lower mantle geothermal gradients of ~0.58 K/km, core mantle boundary temperatures of ~2900°C, bulk Earth molar Mg/Si ratios of ~1.1, intermediate between the chondrite and pyrolite models, and no significant change in mantle composition across the 670-km seismic discontinuity.

Citation: Khan, A., J. A. D. Connolly, and N. Olsen (2006), Constraining the composition and thermal state of the mantle beneath Europe from inversion of long-period electromagnetic sounding data, *J. Geophys. Res.*, *111*, B10102, doi:10.1029/2006JB004270.

1. Introduction

[2] Electrical conductivity reflects chemical composition and physical state of a planet's interior. Studies of minerals at high temperature and pressure indicate that electrical conductivity is thermally activated [*Parkhamenko*, 1982]. Additionally, electrical conductivity varies significantly between minerals and as a function of the composition of individual minerals. Measurements of conductivity therefore hold the potential of providing valuable knowledge about planetary composition and temperature. Obtaining this knowledge requires combining laboratory measurements of the electrical properties of minerals with electrical conductivity profiles derived from geomagnetic field measurements made at the planetary surface. Such an analysis is complicated by uncertainties and lacunae in mineral conductivity data [*Huebner et al.*, 1979; *Shankland*, 1975; *Duba*, 1976] and nonuniqueness inherent in the inversion of electromagnetic sounding data [*Phillips*, 1972; *Parker*, 1980]. However, recent laboratory measurements [e.g., *Katsura et al.*, 1998; *Xu et al.*, 1998a, 1998b; *Xu and Shankland*, 1999; *Xu et al.*, 2000a, 2000b; *Xu and McCammon*, 2002; *Dobson and Brodholt*, 2000a; *Dobson*, 2003] have renewed interest in obtaining convergence between laboratory studies of mineral conductivity and geophysical models derived from electromagnetic induction data [e.g., *Dobson and Brodholt*, 2000b; *Xu et al.*, 2000b; *Ledo and Jones*, 2005]. These studies address whether laboratory-derived mineral conductivities are consistent with a given geophysical model, but because they are based on forward models they cannot explore the range of models that are consistent with the fundamental geophysical observations.

[3] In view of the limitations inherent in forward models, we propose to invert measurements of terrestrial long-period inductive responses, in the form of *C* responses derived by *Olsen* [1999] from a set of geomagnetic observatories in Europe, to constrain thermal state and composition of the Earth's mantle. *C* responses relate the magnetic vertical component to the horizontal gradient of the horizontal components of electromagnetic variations. For a given model configuration that specifies

[1]Niels Bohr Institute, University of Copenhagen, Copenhagen, Denmark.
[2]Earth Sciences Department, Swiss Federal Institute of Technology, Zurich, Switzerland.
[3]Danish National Space Centre, Copenhagen, Denmark.

0148-0227/06/2006JB004270$09.00

the mantle composition and thermal state, the inversion procedure consists of the following steps:

[4] 1. Models of Earth's mantle composition, within the system CaO-FeO-MgO-Al_2O_3-SiO_2 (CFMAS), and geotherm are stochastically generated using a Markov chain Monte Carlo (MCMC) sampling algorithm.

[5] 2. Gibbs free energy minimization is used to compute the mineral modes and densities as a function of depth.

[6] 3. The conductivity profile of the mantle is estimated from the computed mineralogy, by combining it with laboratory-based conductivity models for individual minerals according to an appropriate mixing law.

[7] 4. The geomagnetic response at the Earth's surface, or in space, is then predicted from the trial conductivity profile. The Earth's mass and moment of inertia are estimated from the trial density profile.

[8] 5. The trial configurations geomagnetic response, mass, and moment of inertia are compared to observations to establish whether the configuration is plausible; unsuccessful configurations are rejected and new ones are stochastically generated.

[9] The inverse problem of estimating parameters such as composition and thermal state of the Moon from electromagnetic sounding data, mass and moment of inertia is strongly nonlinear and will be solved using a stochastic based sampling algorithm. The problem is formulated within the Bayesian framework and involves the use of probability density functions (PDFs) to represent every single state of information in the problem [*Tarantola and Valette*, 1982; *Tarantola*, 2004]. The solution to the inverse problem is defined as the conjunction of these PDFs and contained in the posterior PDF. Samples from this posterior PDF are then obtained by employing a MCMC method [e.g., *Mosegaard and Tarantola*, 1995; *Mosegaard*, 1998].

[10] This study, apart from trying to constrain chemical composition and thermal state, serves a deeper purpose, namely that of integrating widely different geophysical data sets into a joint inversion to provide tighter constraints on the internal structure. Geophysical investigations typically invert for a set of parameters that are a priori unrelated. For example, inversion of seismic data give information on seismic wave velocities, and electromagnetic sounding data provide knowledge on the electrical conductivity profile, while gravity data tell us about the subsurface density structure. Using this parameterization there is no obvious way to constrain seismic velocities from inversion of electromagnetic sounding data, for instance, unless, we are in the possession of laboratory measurements or physical laws correlating these particular parameters. By appealing to a set of parameters which are not only common to all data sets, but also characterizes the media under study at a fundamental level we present a way of integrating different geophysical data sets into a joint inversion (Figure 1). The method not only enables us to link the various geophysical data in a natural way it also provides a means of introducing information on various aspects of the media, such as its mineralogy, petrology, geology and geophysics, that can equally serve to correlate the geophysical data in the inversion. The bringing together of geophysics, mineral physics and petrology, or, paraphrased, the direct confrontation of geophysical data with compositional parameters, is the strong point of the method presented here. The method not only enables us to link the various geophysical data in a natural way but also provides a means of introducing information on various aspects of the media, such as its mineralogy, petrology, geology, and geophysics that can equally serve to correlate the geophysical data in the inversion.

2. Laboratory Electrical Conductivity Measurements

[11] Electrical conductivity σ is a thermally activated process and is usually described by an equation of the form

$$\sigma = \sigma_o e^{-E/kT} \tag{1}$$

where σ_o is a constant depending upon the conduction mechanism, E is activation enthalpy, being the sum of the energy required to produce and to move a charge carrier in the structure, T is temperature, and k is Boltzmann's constant. The effect of increasing pressure on electrical conductivity is taken into account through $E = U + pV$, where U is activation energy, p is pressure, and V is activation volume.

[12] Mantle minerals considered here are olivine (Ol), orthopyroxene (Opx), clinopyroxene (Cpx), garnet (Gt), anorthite (An), spinel (Sp), wadsleyite (Wad), ringwoodite (Ring), akimotoite (Aki), C2/c pyroxene (C2/c), magnesiowüstite (Mw), perovskite (Pv), Ca-perovskite (Ca-pv), and postperovskite (Ppv), in accordance with the pyrolite composition of *Ringwood* [1975]. Recent electrical conductivity measurements on most upper and middle mantle minerals (Ol, Opx, Cpx, Gt, Wad, Ring) have converged (see the discussion by *Xu et al.* [2000b]), suggesting that the conductivities of these minerals may be considered to be known with confidence. For the upper and middle mantle minerals (Ol, Opx, Cpx, Gt, Wad, Ring, Aki, and C2/c) we adopt the temperature-dependent conductivity functions summarized by *Xu et al.* [2000b] and compiled in Figure 2. We also employ *Xu et al.*'s [2000b] function for Cpx as a proxy for the conductivities of C2/c pyroxene and akimotoite, as no data are available for these minerals. The experiments used to obtain the conductivity functions were made at oxygen fugacities (fO_2) controlled by the Mo-MoO_2 buffer. However, the effect of fO_2 on mineral conductivity, is poorly quantified, although it has been suggested that olivine could vary as $fO_2^{1/6}$ [*Schock et al.*, 1989; *Duba and Constable*, 1993]. Accordingly, no corrections were made for oxygen fugacity to upper and transition zone mantle minerals. Thus we implicitly assume that oxygen fugacity in and beneath the upper mantle is near to that of the Mo-MoO_2 buffer.

[13] Important lower mantle minerals include Mw and Pv, with Ca-perovskite and postperovskite making up minor amounts. The expected homogeneity of the lower mantle, which is thought to be composed largely of perovskite and magnesiowuestite [*Ringwood*, 1975], requires a model to relate the compositional variations of these phases to their conductivity. Additionally, and in contrast to upper mantle conductivities, extrapolations of experimentally derived conductivity functions to the lower mantle require correction for the effect of pressure [*Shankland et al.*, 1993]. To provide a minimal model for these effects, we assume that the electrical conductivities of Pv and Mw can be repre-

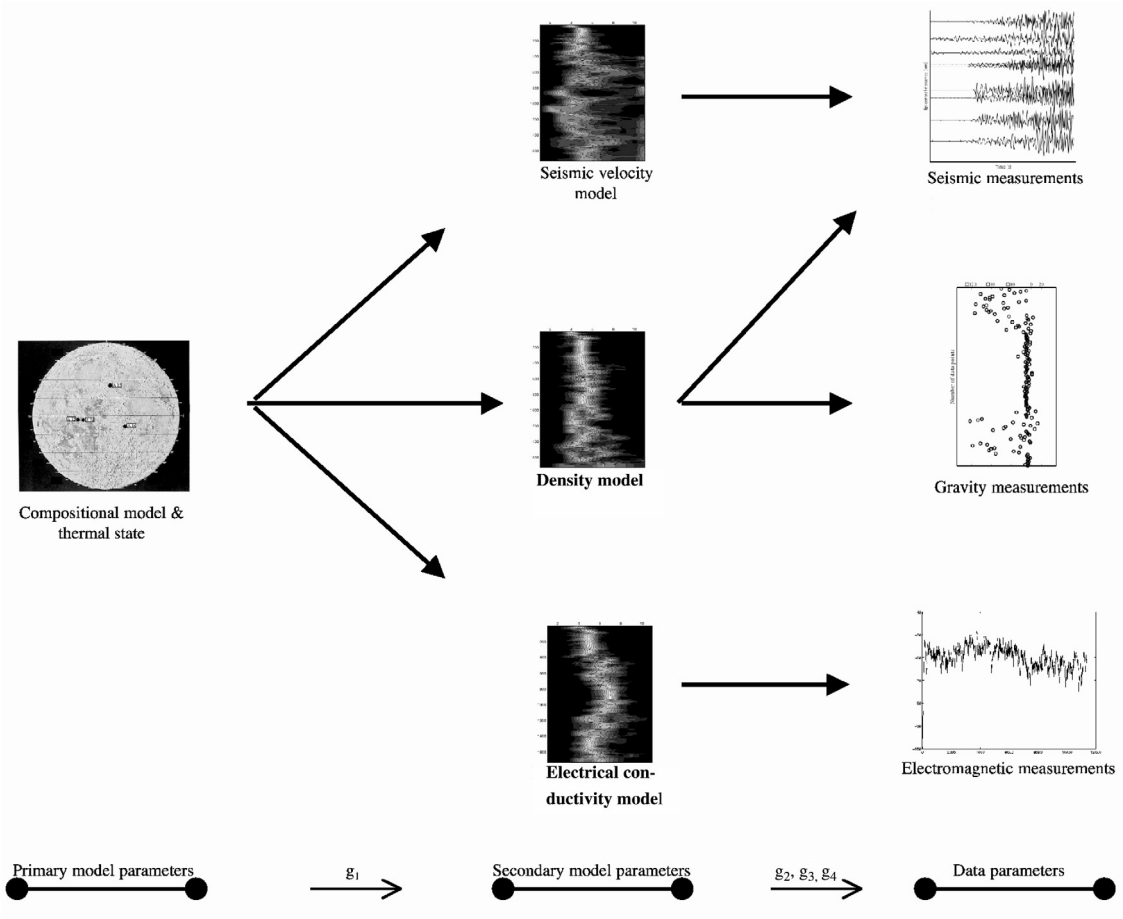

Figure 1. An illustration of the different model and data parameters underlying the description of the geophysical problem. The link between the different model spaces, and thus what links plural geophysical data to petrological and mineralogical parameters, is provided by the different theories (g_1,. . ., g_4) employed in calculating data given the composition and geotherm. Geophysical observations of interest, as exemplified here, could be seismic arrival times, gravity data, and electromagnetic sounding data.

sented by an equation of the general form [*Dobson and Brodholt*, 2000a; *Xu and McCammon*, 2002]

$$\sigma = \sigma_0(x) T^m \exp -[(E + (p - p_o)V)/kT] \quad (2)$$

with

$$\sigma_0(x) = \alpha + \beta x \quad (3)$$

where x is the compositional variable of greatest influence, p is pressure, V is measured activation volume, and m, α, β, and p_o are mineral-specific parameters.

[14] In case of Mw, we use the parameterization suggested by *Dobson and Brodholt* [2000a] for the large polaron conduction mechanism. The experiments by Dobson and Brodholt showed that Mw conductivity is strongly dependent upon x_{Mg} ($=n_{MgO}/[n_{FeO} + n_{MgO}]$), which we adopt as the primary compositional variable in equations (2)–(3). Interpolating the activation energies and preexponential factors derived by Dobson and Brodholt from their experiments with minimal Fe^{3+}, as a function of x_{Mg} yields $m = -0.24$, $\alpha = 10^{12.3}$, $\beta = 10^{10.1}$ at $p_o = 0.1$ GPa. Dobson and Brodholt determined an activation volume of $V = -0.26$ m^{-6}/mol. As the dependence of Mw conductivity on Fe^{3+}/Fe^{2+} (i.e., oxygen fugacity) cannot be accounted for in the context of the CFMAS system our model yields a lower bound for its conductivity.

[15] Alumina solution is the most important chemical substitution influencing the conductivity of perovskite in the CFMAS system [*Duba et al.*, 1979; *Katsura et al.*, 1998; *Xu et al.*, 1998a]. The conductivity of Pv is more complex than Mw, in that both small polaron and ionic conduction mechanisms may be important in perovskite at mantle conditions [*Xu and McCammon*, 2002]. The preexponential terms inferred from experimental observations by *Xu and McCammon* [2002] for Al-free and Al-bearing Pv were used to assess a linear model for the Al dependence of the small polaron mechanism. Combining this model with the activation volume determined by *Goddat et al.* [1999] of -0.13 m^{-6}/mol yields the following parameter values $m = -1$, $\alpha = 10^{3.9}$, $\beta = 10^{20.7}$ at $p_o = 40$ GPa, with x as the mole fraction of alumina relative to silica. The high-temperature conductivity measurements of *Katsura et al.* [1998] are at conditions where the ionic mechanism is expected to dominate, but these experiments show variation with Al content that is similar to that observed for the small polaron mechanism. Accordingly, we assume that ionic and small polaron mechanisms have the same Al dependence.

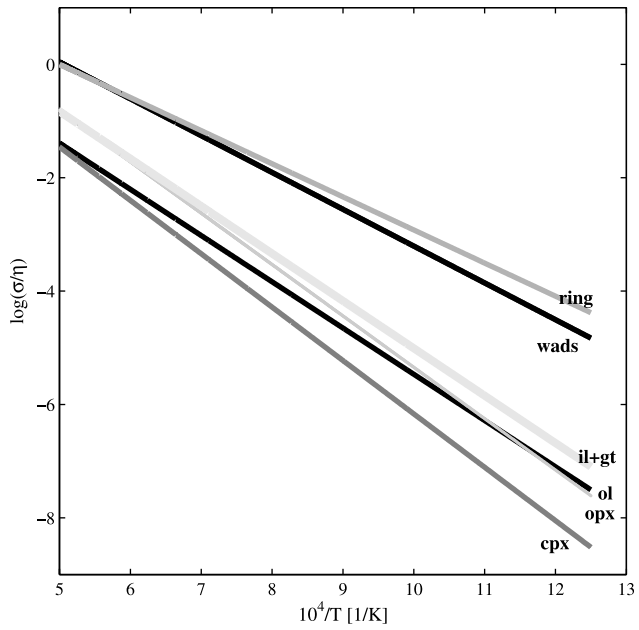

Figure 2. Electrical conductivity as a function of temperature for upper mantle and transition zone minerals considered here (η = 1 S/m).

Following *Xu and McCammon* [2002; *Keys*, 1958], the activation volume of the ionic mechanism is estimated as $4E/K$, where E is activation enthalpy and K is bulk modulus, resulting in the parameter values $V = 0.97$ m^{-6}/mol, $m = -1$, $\alpha = 10^{6.2}$, $\beta = 10^{20.7}$ at $p_o = 25$ GPa.

[16] The electrical conductivities of postperovskite and Ca-perovskite are unknown. Given that alumina is less soluble in Ca-perovskite than it is in perovskite (T. J. Shankland, personal communication, 2005), we take the conductivity of Al-free perovskite (i.e., $x = 0$ in equations (2)–(3)) as a proxy for that of Ca-perovskite. For postperovskite we use the perovskite model, as described above. Ca-perovskite is unlikely to be present in large enough quantities to significantly influence the bulk conductivity [*Xu et al.*, 2000b], whereas postpervoskite, if it is indeed the source of the D″ discontinuity [*Oganov and Ono*, 2004], is present at depths greater than those probed by the soundings used here [*Olsen*, 1999]. Thus the foregoing assumptions are unlikely to be major sources of error for our analysis. The assumption that perovskite and postperovskite have identical conductivity models does not imply, as might be intuitive, that the perovskite to postperovskite transition is transparent to electromagnetic sounding, because Fe is strongly partitioned into postperovskite. As a consequence, provided Mw contributes to the bulk conductivity, the Mw + Ppv assemblage will be significantly less conductive than the overlying Mw + Pv assemblage. Magnesiowüstite and perovskite conductivities are summarized in Figure 3 for various conditions of x, p, and T. As concerns effects of oxygen fugacity on lower mantle minerals, we again follow *Xu et al.* [2000b], who consider fO_2 buffered by Mo-MoO_2 as appropriate in the lower mantle.

3. Mantle Geotherms

[17] The upper mantle geotherm is well constrained from mineral phase transitions. For example, if the 410 and

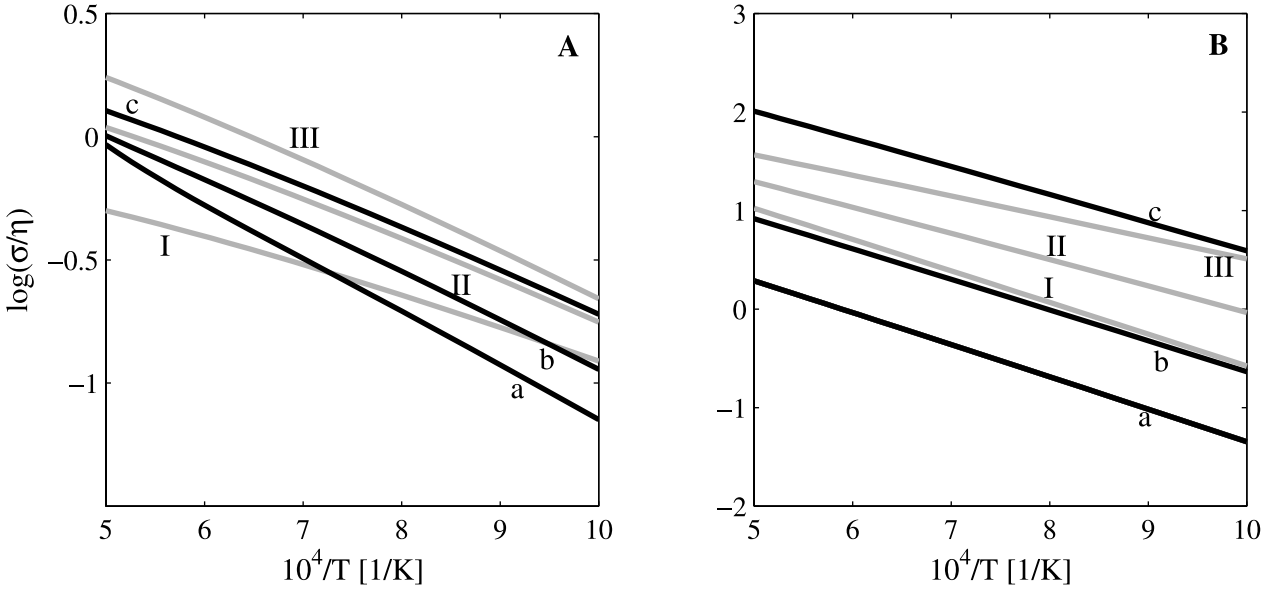

Figure 3. Electrical conductivity of the major lower mantle minerals Mw and Pv at various conditions of x, p, and T using the pressure and compositionally dependent conductivity model detailed in section 2. (a) Conductivity of Pv as function of temperature and composition at a pressure of 113 GPa (line I, $x_{Al} = 0$; line II, $x_{Al} = 0.025$; line III, $x_{Al} = 0.04$) and as a function of temperature and pressure at $x_{Al} = 0.03$ (line a, $p = 50$ GPa; line b, $p = 80$ GPa; line c, $p = 113$ GPa). (b) Conductivity of Mw as function of temperature and composition at a pressure of 20 GPa (line a, $x_{Mg} = 0.95$; line b, $x_{Mg} = 0.895$; line c, $x_{Mg} = 0.8$) and as a function of temperature and pressure at $x_{Mg} = 0.88$ (line I, $p = 10$ GPa; line II, $p = 50$ GPa; line III, $p = 90$ GPa). As before, $\eta = 1$ S/m.

660 km seismic discontinuities correspond to the olivine→β-spinel and γ-spinel→Mw + Pv reactions, then the temperature at these depths can be inferred to be ∼1750 ± 100 K and ∼1900 ± 150 K, respectively [*Ito and Takahashi*, 1989]. However, precious few constraints exist on lower mantle temperatures, where, as noted by *Schubert et al.* [2001], most data are consistent with either hot geotherms, implying layered convection or relatively cold geotherms, indicating whole mantle convection, or any in between these two extremes. Given the sensitivity of electrical conductivity to temperature, laboratory measurements have been turned into possible mantle geotherms through equation (1). Two techniques are traditionally employed, based on inverse and forward modeling approaches, respectively. Whereas the former inverts electromagnetic sounding data to obtain the conductivity structure which can then be compared with laboratory measurements for candidate minerals [e.g., *Constable*, 1993], the latter models geomagnetic responses measured at several observatories based on estimated geotherms and measured mineral electrical conductivities [e.g., *Dobson and Brodholt*, 2000b]. In the study of Dobson and Brodholt it was found that either cool or hot mantle geotherms are consistent with data, depending on whether the lower mantle is composed of Al-free or Al-bearing Pv, because of the increased electrical conductivity of the Al-bearing Pv phase. On the basis of the results obtained by *Xu et al.* [1998b], who found that the conductivity of Pv containing 2.9 wt % Al_2O_3 increased by a factor of about 3 over that of Al-free Pv, Dobson and Brodholt favored a cool mantle geotherm, as Al is a significant constituent of the lower mantle.

4. Inverse Problem: Theoretical Preliminaries

4.1. Statement and Solution of the Inverse Problem

[18] This section will only capture the essentials of the Bayesian formulation of the general inverse problem and the methods underlying the Markov chain Monte Carlo (MCMC) algorithm. For an in-depth analysis the reader is referred to *Tarantola and Valette* [1982], *Mosegaard and Tarantola* [1995], *Mosegaard* [1998], and *Tarantola* [2004].

[19] Using a probabilistic inference approach to combine the information describing the various aspects of the problem, the solution to the general inverse problem is defined as

$$\sigma(\mathbf{m}) = k\eta(\mathbf{m})\mathcal{L}(\mathbf{m}) \tag{4}$$

where k is a normalization constant, $\eta(\mathbf{m})$ is the prior probability density function (PDF), and $\mathcal{L}(\mathbf{m})$ is the likelihood function, which in probabilistic terms can be interpreted as a measure of how well a given model $\mathbf{m}$ fits the observed data; $\sigma(\mathbf{m})$ is known as the posterior PDF and contains all the information about our parameterized physical system.

4.2. Sampling the Posterior Distribution

[20] To obtain information from the model space, the basic idea is to design a random walk that samples some initial probability distribution. By subsequently applying a probabilistic rule, we can modify the random walk in such a way that the random walk will sample some target distribution. An algorithm that is capable of generating points x_i in the parameter space with prior probability η_i, and that allows evaluation of the likelihood function of any parameter vector, can be used to sample the posterior probability density in the model space. The Metropolis-Hastings algorithm [*Metropolis et al.*, 1953; *Hastings*, 1970], which is a Markov chain Monte Carlo (MCMC) method, can be shown to be the one that most efficiently achieves this goal.

[21] **Algorithm:** Given a random function $\Omega(\mathbf{m}^n)$ sampling the prior probability density $\eta(\mathbf{m})$ if applied iteratively $\mathbf{m}^{n+1} = \Omega(\mathbf{m}^n)$ and given additionally a random function $\mathcal{U}$ generating a uniformly distributed random number from the interval [0,1], the random function Γ, which iteratively operates on the current parameter vector $\mathbf{m}^n$ and produces the next parameter vector $\mathbf{m}^{n+1}$

$$\mathbf{m}^{n+1} = \Gamma(\mathbf{m}^n) = \begin{cases} \Omega(\mathbf{m}^n) & \text{if } \mathcal{U} \le \min\left[1, \dfrac{\mathcal{L}(\Omega(\mathbf{m}^n))}{\mathcal{L}(\mathbf{m}^n)}\right], \\ \mathbf{m}^n & \text{else.} \end{cases}$$

samples the probability density $\sigma(\mathbf{m}) = k\eta(\mathbf{m})\mathcal{L}(\mathbf{m})$.

[22] In addition, Ω has to satisfy the following two constraints: (1) given enough iterations, access to all points $\mathbf{m}$ in the parameter space must be ensured through the iterative procedure and (2) successive visits (or more) to the same point are possible, i.e., $\mathbf{m}^n = \Omega(\mathbf{m}^n)$.

[23] The advantage of using this algorithm to sample the posterior PDF is that sampling is concentrated in areas of the model space where parameter vectors consistent with data as well as prior information exist. Furthermore, resolution measures (means, covariances, etc.) can easily be evaluated from

$$\mathcal{R}(\Lambda, f) = \int_\Lambda f(\mathbf{m})\sigma(\mathbf{m})d\mathbf{m} \approx \frac{1}{N}\sum_{\{n|\mathbf{m}_n\in\Lambda\}} f(\mathbf{m}_n) \tag{5}$$

where $f(\mathbf{m})$ is a given function of the model parameters $\mathbf{m}$, Λ is an event or subset of the model space containing the models of current interest, and N is the total number of samples taken from Λ.

5. Constructing the Forward Model

[24] The purpose here is to determine the Earth's mantle composition and thermal state from electromagnetic transfer functions, mass and moment of inertia. Reversing this order, that is, predicting the geophysical observations from a knowledge of the composition and thermal state of the Earth is thus what is meant by solving the forward problem. This statement is usually condensed into the expression

$$\mathbf{d} = \mathrm{g}(\mathbf{m}) \tag{6}$$

where g is a (usually nonlinear) functional relation governing the physical laws that relate model and data, expressing our mathematical model of the physical system under study. Let us break equation (6) up into a number of forward modeling sequences

$$\begin{array}{ccccc} & & \mathbf{m}_2 & \xrightarrow{\mathrm{g}_2} & \mathbf{m}_3 \xrightarrow{\mathrm{g}_3} \mathbf{d}_1 \\ & \overset{\mathrm{g}_1}{\nearrow} & & & \\ \mathbf{m}_1 & & & & \\ & \underset{\mathrm{g}_1}{\searrow} & & & \\ & & \mathbf{m}_4 & \xrightarrow{\mathrm{g}_4} & \mathbf{d}_2 \end{array}$$

where $\mathbf{m}_1$ is an assumed starting composition and geotherm, g_1 is the forward operator embodying the Gibbs free energy minimization routine, calculating mineral phase proportions (modal mineralogy) and their physical properties, in the form of the density, and contained in the model parameter vectors $\mathbf{m}_2$ and $\mathbf{m}_4$, respectively. g_2 embodies the combination of modal mineralogies with laboratory electrical conductivity measurements and an appropriate mixing law, $\mathbf{m}_3$ contains the bulk conductivity model, g_3 is the physical law connecting the electrical conductivity profile to the electromagnetic transfer functions ($\mathbf{d}_1$), and finally g_4 is the operator that calculates mass and moment of inertia, contained in the data vector $\mathbf{d}_2$. Note that we have not made the distinction between model parameters and data parameters, as there is no conceptual distinction between the two. Before delineating the different forward modeling operators let us briefly describe our physical model of the Earth.

[25] We assume a spherically symmetric model of the Earth, which is divided into four concentric shells of variable thickness. The layers correspond to crust, upper mantle, lower mantle, and core. The outermost shells are described by the model parameters: thickness d, composition c, and temperature T. The physical properties of the core are specified by the model parameters: size, density, and electrical conductivity. The simplification for the core layer was made because we lack the thermodynamic data required to model metallic compositions. Temperature T is defined at 26 unequally spaced fixed nodes. To determine the mineralogical structure and corresponding mass density, it is also necessary to specify the pressure profile. For this purpose the pressure is obtained by integrating the load from the surface (boundary condition $p = 10^5$ Pa).

5.1. Solving the Forward Problem I: Thermodynamical Modeling

[26] Possible mantle compositions were explored within the system CaO-FeO-MgO-Al_2O_3-SiO_2. The mantle mineralogy is assumed to be dictated in general by thermodynamic equilibrium, in which case the composition and proportions of the mantle phases are those that minimize the Gibbs energy of the system

$$G^{\mathrm{sys}} = \sum_{i=1}^{\Pi} n^i G^i\left(x_1^i, \ldots, x_{c-1}^i\right) \tag{7}$$

subject to the physical constraints

$$n^i \geq 0 \tag{8}$$

and

$$n_j^{\mathrm{sys}} = \sum_{i=1}^{\Pi} n^i x_i^j, \; j = 1, \ldots, c, \tag{9}$$

where Π is the total number of phases that may occur in the system, as opposed to those which are actually stable; $G^i(x_1^i,\ldots,x_{c-1}^i)$ is the Gibbs energy of an arbitrary quantity, here chosen to be a mole, of the ith phase; n^i is amount of the phase; c is the number of independently variable kinds of matter in the system, i.e., the chemical components, x_i^j is the concentration of the jth component in the ith phase; and n_j^{sys} is the amount of the component in the system. In general, because of the dependence of the Gibbs energy of a phase on its composition, equations (7)–(9) pose a nonlinear optimization problem that is both costly and difficult to solve. To circumvent this difficulty, the continuous functions $G^i(x_1^i,\ldots, x_{c-1}^i)$ are represented by points $G_1^{i_1}(x_1^{i_1},\ldots, x_{c-1}^{i_1})\ldots G_k^{i_k}(x_1^{i_k},\ldots, x_{c-1}^{i_k})$ obtained by evaluating $G^i(x_1^i,\ldots,x_{c-1}^i)$ at k arbitrarily chosen compositions. Equations (7)–(9) reformulated in terms of these points then pose a linear optimization problem which is solved by the Simplex algorithm [*White et al.*, 1958] using a computer program described by *Connolly* [2005]. The accuracy of the linearized formulation is determined by the discretization of the continuous functions $G^i(x_1^i,\ldots,x_{c-1}^i)$. Here this discretization was done to resolve phase compositions with an accuracy of better than 2%.

[27] The equilibrium assumption is dubious at low temperature [e.g., *Wood and Holloway*, 1984]. In recognition of this limitation, if a model required a mineralogy at a temperature below 800 K, then the equilibrium mineralogy was calculated at 800 K. Thermodynamic properties were then computed for the assemblage so obtained at the temperature of interest.

[28] The nonstoichiometric phases considered in the Gibbs energy minimization procedure are summarized in Table 1, and in addition, stishovite and calcium perovskite were considered as stoichiometric phases. Thermodynamic properties at pressure and temperature were computed using the equation of state proposed by *Stixrude and Bukowinski* [1990] with parameters as given in *Stixrude and Lithgow-Bertelloni* [2005a]. This formulation employs the Debye model to account for the temperature dependence of the Helmholtz energy and specifically assumes the Debye temperature to be

$$\theta = \theta_0 \exp\left\{ \gamma_0 \frac{\left[1 - \left(\frac{V}{V_0}\right)^q\right]}{q} \right\} \tag{10}$$

where γ and V are the Grüneisen thermal parameter and volume, respectively, q is a constant, and the subscript zero denotes properties at the reference conditions (0 GPa, 300 K). For mid-to-lower mantle conditions, the data of Stixrude and Lithgow-Bertelloni were augmented by the end-member data for wuestite, magnesio-postperovskite, calcium perovskite, the ferrous and aluminous perovskite and postperovskite end-members (Table 2). The properties of wuestite and the perovskite end-member properties were derived from the equation of state parameterized by *Fabrichnaya* [1998], with θ adjusted to match the third law entropy at 20 GPa and 1600 K, and q taken to be identical to the value of the isostructural end-member in Stixrude and Lithgow-Bertelloni's compilation. The Helmoltz energy of wuestite was estimated by fitting the phase relations observed by *Irifune* [1994] for a pyrolite bulk composition at 1873 K and 28.5 GPa. For calcium-perovskite, elastic constants are from *Karki and Crain* [1998], γ_0 and η_{S0} are approximated by the corresponding values for magnesio-perovskite [*Stixrude and Lithgow-Bertelloni*, 2005a], and the Helmoltz energy and Debye temperature are adjusted to place the equilibrium diopside with wadsleyite, stishovite, and calcium perovskite at 18.15 GPa and 1873 K with a Clapeyron

Table 1. Solution Notation, Formulae, and Model Sources[a]

Symbol	Solution	Formula	Source
Cpx	clinopyroxene	$Ca_{2y}Mg_{4-2x-2y}Fe_{2x}Si_4O_{12}$	1
Gt	garnet	$Fe_{3x}Ca_{3y}Mg_{3(1-x+y+z/3)}Al_{2-2z}Si_{3+z}O_{12}$, $x + y \leq 1$	1
Ol	olivine	$[Mg_xFe_{1-x}]_2SiO_4$	1
Opx	orthopyroxene	$[Mg_xFe_{1-x}]_{4-2y}Al_{4(1-y)}Si_4O_{12}$	1
Sp	spinel	$Mg_xFe_{1-x}Al_2O_3$	1
C2/c	pyroxene	$[Mg_xFe_{1-x}]_4Si_4O_{12}$	1
Aki	akimotoite	$[Mg_xFe_{1-x}]_{1-y}Al_{2y}Si_{1-y}O_3$	2
Pv	perovskite	$[Mg_xFe_{1-x}]_{1-y}Al_{2y}Si_{1-y}O_3$	2
Ppv	postperovskite	$[Mg_xFe_{1-x}]_{1-y}Al_{2y}Si_{1-y}O_3$	3
Ring	ringwoodite	$[Mg_xFe_{1-x}]_2SiO_4$	1

[a]Unless otherwise noted, the compositional variables x, y, and z may vary between zero and unity and are determined as a function of the computational variables by free-energy minimization. Sources are 1, *Stixrude and Lithgow-Bertelloni* [2005a]; 2, *Fabrichnaya* [1998]; and 3, *Ono and Oganov* [2006] (refer to text for additional details).

slope of 2.08 MPa/K, after the experimentally determined phase relations of *Akaogi et al.* [2004]. For magnesio-postperovskite, elastic constants are from *Oganov and Ono* [2004] and *Ono and Oganov* [2006] or approximated by those inferred for perovskite [*Stixrude and Lithgow-Bertelloni*, 2005a], and the Helmoltz energy is chosen to locate the magnesio-perovskite to magnesio-postperovskite transition at 130 GPa and 2500 K with a Clapeyron slope of 8.0 MPa/K, as consistent with the "thermodynamic" model of *Ono and Oganov* [2006]. Excess enthalpies for non-stoichiometric magnesiowuestite and perovskite solutions were computed from a second-order Margules expansion. In both cases interaction terms were approximated from the excess functions calibrated by *Fabrichnaya* [1998] evaluated at 20 GPa and 1600 K. The effect of iron and aluminum solution in the postperovskite phase was accounted for by ferrous and aluminous postperovskite end-members whose properties differ from magnesio-postperovskite by a constant energy difference that was calibrated (Table 2) from the perovskite postperovskite distribution coefficients computed by *Ono and Oganov* [2006] at 4000 K and 120 GPa. This treatment is equivalent to assuming Henry's law solution behavior that is independent of pressure and temperature for all conditions of interest.

[29] The CFMAS chemical model is thought to account for more than 98% of the mass of the Earth's mantle [e.g., *Irifune*, 1994], and it has been argued to provide an adequate model for the mantle seismic [e.g., *da Silva et al.*, 2000] and electrical conductivity structure [e.g., *Xu et al.*, 2000b]. Components not considered include Cr_2O_3, NiO, MnO, and TiO_2, and make up approximately 2 wt % of typical peridotitic compositions [*Irifune*, 1994].

5.2. Solving the Forward Problem II: Modeling Bulk Mantle Conductivity

[30] Having determined the minerals present, their abundances and their electrical conductivities, the bulk rock electrical conductivity can be calculated given knowledge of the geometrical distributions of the minerals. However, as rocks are inhomogeneous due to their mixed mineral content, information on texture is not available and macroscopic mixture theory is used instead. The theory of mixtures is broadly organized into three general categories, including exact results, bounds and estimates [e.g., *Guéguen and Palciuskas*, 1994; *Berryman*, 1995]. What is usually done in the absence of information on the geometrical distribution of individual mineral phases is to consider possible conduction models for a material in which the most abundant coexisting phases are distributed homogeneously. Several estimates and bounds can be calculated, including series and parallel solutions [*Schulgasser*, 1976], Hashin-Shtrikman bounds [*Hashin and Shtrikman*, 1962], effective medium theories [*Landauer*, 1952], geometric means [*Shankland and Duba*, 1990], and Voigt-Reuss-Hill averages [*Watt et al.*, 1976]. However, as *Xu et al.* [2000b] showed that variations between calculated conductivities using the various averaging schemes are of the order of 0.1 log unit or less (see also *Shankland and Duba* [1990] for a discussion), we shall limit ourselves to using the geometric mean as an estimator,

$$\sigma(r) = \sigma_{GM}(r) = \prod_i \sigma_i^{x_i(r)}(r)(x, p, T)$$

where $x_i(r)$ is volume fraction as a function of radius and σ_i is the conductivity of phase i. We neglect contributions which might arise from the presence of grain boundaries, porosity, melt and water, as these are thought to represent only a small fraction of the bulk conductivity at the high pressures prevailing in the Earth's mantle [*Xu et al.*, 2000b].

5.3. Solving the Forward Problem III: Estimating Transfer Functions for a Spherically Symmetric Conductivity Model

[31] Estimating a set of transfer functions from the electrical conductivity structure of a layered sphere with

Table 2. End-Member Parameters Used to Augment the Thermodynamic Data Compiled by *Stixrude and Lithgow-Bertelloni* [2005a][a]

End-Member	Phase	Formula	A_0, kJ/mol	V_0, cm^3/mol	K_0, GPa	K'_0	θ_0, K	γ_0	q	G_0, GPa	G'_0	η_{S0}
Calcium-perovskite		CaO	−68.1	27.3	241.0	4.1	842.0	1.5	1.0	164.0	1.9	4.0
Ferro-akimotoite	Aki	$FeSiO_3$	5.4	27.6	199.9	4.0	659.0	1.6	*1.7*	132.0	*1.6*	*2.9*
Corundum	Aki	Al_2O_3	6.6	25.58	251.9	4.2	949.0	1.27	*1.7*	132.0	*1.6*	*2.9*
Magnesio-postperovskite	Ppv	$MgSiO_3$	66.6	24.03	250.1	4.0	891.0	1.56	0.9	194.0	1.7	4.0
Ferro-postperovskite	Ppv	$FeSiO_3$	148.4	*24.03*	*250.1*	*4.0*	*891.0*	*1.56*	*0.9*	*194.0*	*1.7*	*4.0*
Alumino-postperovskite	Ppv	Al_2O_3	157.2	*24.03*	*250.1*	*4.0*	*891.0*	*1.56*	*0.9*	*194.0*	*1.7*	*4.0*
Ferro-perovskite	Pv	$FeSiO_3$	38.0	25.59	272.5	4.0	682.0	2.37	*1.0*	*177.0*	*1.7*	*4.0*
Alumino-perovskite	Pv	Al_20_3	110.6	24.0	262.5	4.1	766.0	1.8	*1.0*	*177.0*	*1.7*	*4.0*
Wuestite	Mw	FeO	26.0	12.25	178.3	4.0	328.0	1.57	*1.7*	*131.0*	*2.2*	*2.3*

[a]Data are derived as discussed in the text. A is the Helmholtz energy; K_0, G_0, K'_0, and G'_0 are the adiabatic bulk and shear moduli and their pressure derivatives, respectively; and η_S is the shear-dependent part of the finite strain generalization of the Gruneisen parameter (γ_0). Other parameters are defined in reference to equation (4). Parameters in italics are approximated by the properties of the isostructural end-member listed by *Stixrude and Lithgow-Bertelloni* [2005a].

Table 3. Apparent Resistivities ρ_a and Phases ϕ for 23 Periods T, Including Their Uncertainties, Obtained by Averaging Results From 42 European Observatories[a]

T, s	ρ_a, Ω m	ϕ, deg
	11 Year and Long Period	
346,896,000	0.11 ± 0.05	86.7 ± 12.6
31,536,000.	0.66 ± 0.01	74.8 ± 2.2
15,768,000.	0.85 ± 0.24	67.5 ± 4.1
10,512,000.	1.99 ± 0.49	70.3 ± 3.5
6,307,200.	2.43 ± 0.47	69.8 ± 2.8
3,942,000.	2.74 ± 0.69	69.8 ± 3.6
2,866,909.	3.41 ± 0.82	67.8 ± 3.4
2,102,400.	4.02 ± 0.95	72.7 ± 3.4
	Dst	
2,592,000.	3.41 ± 0.29	72.4 ± 1.5
1,296,000.	6.11 ± 0.50	70.6 ± 1.5
864,000.	8.15 ± 0.39	71.4 ± 0.9
518,400.	11.20 ± 1.06	73.9 ± 1.7
324,000.	16.32 ± 1.59	76.1 ± 1.7
235,636.	21.36 ± 2.67	72.4 ± 2.2
172,800.	27.45 ± 4.42	72.1 ± 2.9
	S	
86,400.	39.33 ± 5.49	66.7 ± 2.6
43,200.	56.2 ± 10.3	62.6 ± 3.5
28,800.	67.5 ± 11.1	57.5 ± 3.2
21,600.	76.4 ± 11.1	54.7 ± 2.9
17,280.	83.4 ± 14.0	49.4 ± 3.3
14,400.	91.3 ± 16.6	46.6 ± 3.7
12,343.	94.4 ± 19.5	45.6 ± 4.2
10,800.	86.1 ± 20.2	46.1 ± 4.7

[a]For a discussion of uncertainties the reader is referred to *Olsen* [1998, 1999]. The values for the 11 year period are from *Harwood and Malin* [1977]. *S* denotes the period range appropriate for geomagnetic daily variations, while *Dst* covers the period range up to several days.

variable piecewise constant conductivity is a well-known problem in the study of electromagnetics, thus obviating a repetition of a detailed derivation (the reader is referred to, e.g., *Srivastava* [1966], *Banks* [1969], *Schmucker* [1970], and *Parkinson* [1983] for more details).

[32] For the present purposes we imagine the Earth to be made up of a set of concentric shells each with constant conductivity. The induction equation, $\nabla^2\mathbf{B} = k^2\mathbf{B}$, where $\mathbf{B}$ is the magnetic field vector and k wave number, must then be solved within each shell and in the spherical central region. The jth shell is assumed to extend from r_j to r_{j-1} with conductivity σ_j and wave number $k_j^2 = -i\omega\mu\sigma_j$, where ω is frequency and μ permeability. We assume that the primary (inducing) field is given by a potential of the form

$$V_e = B_e \frac{r^n}{a^{n-1}} S_n^m(\theta,\phi) e^{-i\omega t}, \tag{11}$$

where B_e is a complex number representing the external physical magnetic field component at frequency ω, r is radius, a, radius of the Earth, S_n^m is a surface spherical harmonic of degree n and order m, ω denotes cyclic frequency and t is time. Solving the induction equation then gives us the magnetic field components in the jth shell. Outside the sphere, the field can be expressed by a scalar potential of primary and secondary fields

$$V = a\left[B_e\left(\frac{r}{a}\right)^n + B_i\left(\frac{a}{r}\right)^{n+1}\right] S_n^m(\theta,\phi) e^{-i\omega t} \tag{12}$$

where B_i denotes a complex number representing the internal physical magnetic field component at frequency ω. These can then be used to determine the ratio of internal to external magnetic fields (the transfer function Q) at the surface. Apparent resistivities and phases are related to the C response via the relations $\rho_a = \omega\mu_o|C|^2$ and $\phi = \pi/2 + \arg\{C\}$, where the transfer function Q is determined by the C response [*Schmucker*, 1970]

$$C_n(\omega) = \frac{a}{n+1}\,\frac{1 - \frac{n+1}{n}Q_n(\omega)}{1 + Q_n(\omega)} \tag{13}$$

In summary, given a one-dimensional (1-D) conductivity structure $\sigma(r)$, that is, a conductivity model which only depends on radius, we can use equation (13) above to determine transfer functions at various frequencies and compare these to the observed transfer functions. Also, we assume that $n = 1$.

[33] The data considered here include the C responses derived by *Olsen* [1999] by using time series of daily mean values of 50 years of data for periods between 1 month and 1 year collected from 42 observatories. Derivation of C responses (and their uncertainties) from long-period geomagnetic observatory variations are described by *Olsen* [1998]. The C responses in the form of apparent resistivity and phase as well as associated uncertainties are summarized in Table 3.

5.4. Solving the Forward Problem IV: Mass and Moment of Inertia

[34] Once the bulk density as a function of depth has been calculated we estimate mass and moment of inertia using the simple relations

$$I = \frac{8\pi}{3}\int \rho(r) r^4 dr, \qquad M = 4\pi \int \rho(r) r^2 dr \tag{14}$$

Values adopted for Earth's averaged mass (M) and moment of inertia (I) are $5.97 \pm 0.01 \times 10^{24}$ kg and 0.33 ± 0.001 I/MR^2, respectively, where R is the mean radius of the Earth (6371 km) [*Yoder*, 1995].

6. Solving the Inverse Problem

6.1. Parameterization of the Problem and Sampling the Prior Distribution

[35] As noted, we model the Earth as consisting of four layers corresponding to crust, upper mantle, lower mantle, and core. The layers are of variable thickness d and are assumed to be uniformly distributed within the intervals $d_{\text{crust}} \in [5;35$ km$]$, $d_{\text{UM}} \in [d_{\text{crust}}; r_{\text{surface}} - r_{\text{core}}]$, where d_{UM} is the thickness of the upper mantle layer, r_{surface} is radius of the Earth and r_{core} is core radius, the latter two anchored at 3480 km and 6371 km, respectively. The core is parameterized further by its density (ρ_{core}) and bulk electrical conductivity (σ_{core}). These are also distributed uniformly in the intervals, $\rho_{\text{core}} \in [\rho_m; \rho_c]$, where ρ_m is the value of ρ at the base of the mantle and $\rho_c = 13$ g/cm^3 and $\sigma_{\text{core}} \in [\sigma_m; \sigma_c]$, where σ_m is likewise the electrical conductivity at the base of the mantle and $\sigma_c = 10^5$ S/m, which is reasonably close to the value of 5×10^5 S/m determined by *Stacey and Anderson* [2001].

[36] In contrast to the core, the silicate layers are parameterized by the composition c in the chemical system

CaO-FeO-MgO-Al_2O_3-SiO_2. The oxide proportions are log-uniformly distributed within the intervals CaO $\in$ [1; 8], FeO $\in$ [5; 20], MgO $\in$ [33; 55], $Al_2O_3 \in$ [1; 8] and $SiO_2 \in$ [20; 55] (all in wt %), and with the normalization constraint in each layer $\sum_i c_i = 100$ wt %.

[37] Temperature T is evaluated at 26 nodes at intervals of 50 km down to a depth of 1000 km, which were increased to 500 km in the depth range from 1000 km down to the core-mantle boundary (CMB). Rather than perturbing T directly, we perturb dT/dz, where z is depth, by assuming three variable thermal gradients to exist in the crust, upper, and lower mantle. Temperatures are then changed according to the following scheme: $T_k = T_{k-1} + (a_i + b_i \cdot \alpha)(z_k - z_{k-1})$, where $a_{i=1,\ldots,3} = 6, 2, 0.3$°C/km and $b_{i=1,\ldots,3} = 5, 1, 0.4$°C/km and α is a uniformly distributed random number in the interval [0; 1]. A mantle adiabat for a potential temperature of approximately 1200°C, computed from the thermodynamic model assuming a pyrolitic bulk composition [*Ringwood*, 1966], was used as a lower bound on nodal temperatures. Surface temperature is held constant at 0°C.

[38] The thermodynamic and electrical conductivity models detailed previously are used to establish the mineralogy, density and conductivity within the silicate layers (at intervals of 50 km for the depth range 6371–5371 km and intervals of 200 km for the range 5371–3480 km) from the surface downward as a function of pressure, temperature, and composition.

6.2. Sampling the Posterior Distribution

[39] Under the assumption that data noise is gaussian distributed, and that observational uncertainties and calculation errors are independent among the different geophysical methods employed, the likelihood function can be written as

$$\mathcal{L}(\mathbf{m}) \propto \exp\left(- \sum_i \frac{\left[d^{\rho_a^i}_{\mathrm{obs}} - d^{\rho_a^i}_{\mathrm{cal}}(\mathbf{m})\right]^2}{2\varepsilon_i^2} - \sum_j \frac{\left[d^{\phi_j}_{\mathrm{obs}} - d^{\phi_j}_{\mathrm{cal}}(\mathbf{m})\right]^2}{2\varepsilon_j^2} - \frac{\left[d^{M}_{\mathrm{obs}} - d^{M}_{\mathrm{cal}}(\mathbf{m})\right]^2}{2\varepsilon_M^2} - \frac{\left[d^{I}_{\mathrm{obs}} - d^{I}_{\mathrm{cal}}(\mathbf{m})\right]^2}{2\varepsilon_I^2} \right) \quad (15)$$

where d_{obs} denotes observed data, with superscripts alluding to the particular geophysical observation, $d_{\mathrm{cal}}(\mathbf{m})$ denotes calculated data, and ε denotes the uncertainty on either of these.

[40] In each iteration a shell was chosen at random, and subsequently, all parameters pertaining to this shell were perturbed using the proposal (prior) distribution as defined in section 6.1. The adopted proposal distribution has a burn-in time of the order of 1×10^4 iterations after which retention of samples commences. In all 1 million models were sampled and to ensure near-independent samples every 100th model was retained for further analysis, with an overall acceptance rate of 35%. Generally, we are plotting prior PDFs next to posterior PDFs as a comparison of the two provides us with an indication of the amount of information contained in the data.

[41] In relation to the inverse problem, we chose a general approach in solving it. The advantage of the probabilistic approach lies in its inherent ability to fully incorporate nonlinearities into the final solution, obviating any form of linearization of the original problem and thus providing more realistic error limits to the results for a given resolution. In solving inverse problems, we face the usual trade-off between resolution and uncertainty, which is largely determined by the chosen parameterization. Presently, we chose to model the Earth using three compositional layers and this was based on a choice of parsimony. The resolution adopted here was found on the grounds that the distribution of calculated data provided an adequate fit to the observed data distribution. More complex models could equally well have been chosen, although at the expense of increasing model parameter uncertainties. Having said this, it is clear that the probabilities which we have calculated here are mathematical entities that are based on the quantitative information which has been used as input in the inversion. Stated differently, the probabilities that we calculate are based entirely on (1) data and their uncertainties, (2) prior information as quantified here, and (3) the physical relation between data and unknown model parameters.

7. Results

[42] As our model of the Earth is based on spherical symmetry, we are restricted to considering 1-D radial profiles. Possible contributions from crustal heterogeneity [*Garland*, 1981; *Evans et al.*, 1999] are disregarded as the long-period data considered here are not sensitive to the crust (*Olsen* [1999] considers penetration depths starting at ~200 km).

7.1. Predicted Data

[43] Calculated mass and moment of inertia values as well as apparent resistivities and phase angles are shown in Figures 4 and 5 together with observed data. The significance of data is apparent as it provides the mechanism by which the prior PDF is changed into the posterior PDF. This is apparent as a significant narrowing of the prior PDF (Figures 4a and 4b).

7.2. Composition, Temperature, Mantle Discontinuity and Mineralogy

[44] Upper and lower mantle prior and posterior compositions are displayed in Figure 6. From these are constructed upper and lower mantle Mg/Si ratios, which are shown in Figure 7. Prior and posterior geotherms are displayed in Figure 8. Upper mantle geotherms are in good agreement with temperature constraints derived from laboratory mineral phase transitions (see section 3). As already mentioned, *Dobson and Brodholt* [2000b] combined recent laboratory electrical conductivity measurements with the geotherms of *Brown and Shankland* [1981], representative of whole mantle and layered convection end-members, to produce synthetic electrical conductivity models which were used to estimate (forward model) the global average C responses of *Constable* [1993]. The response functions of Constable are valid for periods of 3.5 days to 4 months and thus do not sense the mantle to depths possible with the present data set. Dobson and Brodholt argued that if the lower mantle consists of Al-bearing perovskite, then it must be cool, whereas a lower mantle made up of Al-free perovskite would be hot. On the basis of a pyrolitic model, Dobson

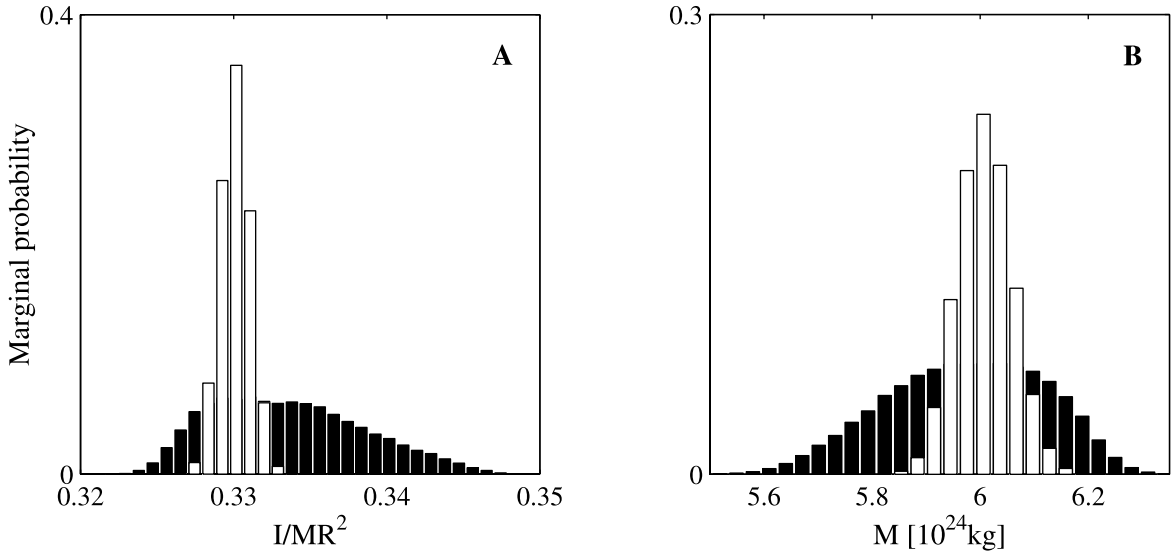

Figure 4. Prior (black bars) and posterior (white bars) data fit. A simple comparison of prior and posterior provides us with a measure of how much information is contained in the data. The extreme narrowing of the posterior data distribution clearly indicates this in case of both (a) moment of inertia and (b) mass.

and Brodholt infer Al contents of ~4 wt % and favor a cool geotherm. The reduced Al contents inferred here for the lower mantle require somewhat higher mantle temperatures. Our inferred CMB temperatures agree with those obtained by *Stixrude and Lithgow-Bertelloni* [2005b], who, removing boundary layer effects and using the adiabat of *Stacey* [1977], estimate a temperature at the CMB of 3015 K. By additional extrapolation to the surface they obtained a temperature of 1573 K.

[45] Sampled depth to the upper/middle mantle transition is displayed in Figure 9 and is seen to be almost flat down to 1500 km depth. This result, together with the broadly overlapping upper and lower mantle compositions derived here, suggests that no significant large-scale heterogeneities exist in the mantle. This is further supported by the obtained Mg/Si ratios, which indicate compositional trends that lie in between that of pyrolite and chondrite and generally agree with estimates of the bulk silicate Earth composition

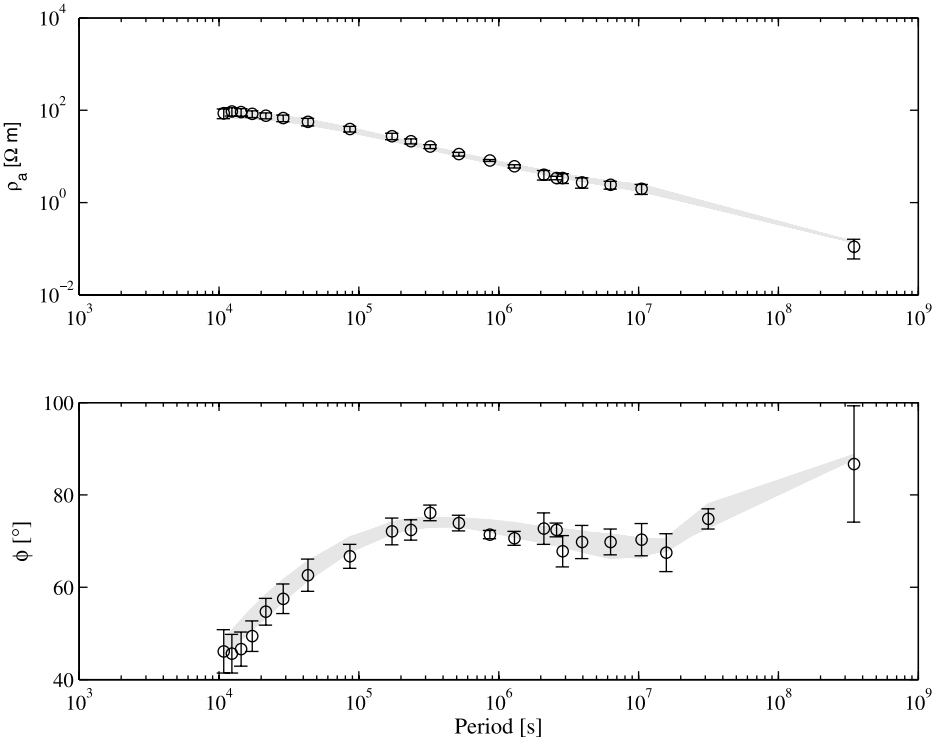

Figure 5. Posterior fit of electromagnetic sounding data. (top) Predicted apparent resistivity values (gray lines) with the observations [*Olsen*, 1999], including error bars, superimposed. (bottom) Calculated phase angles and observations.

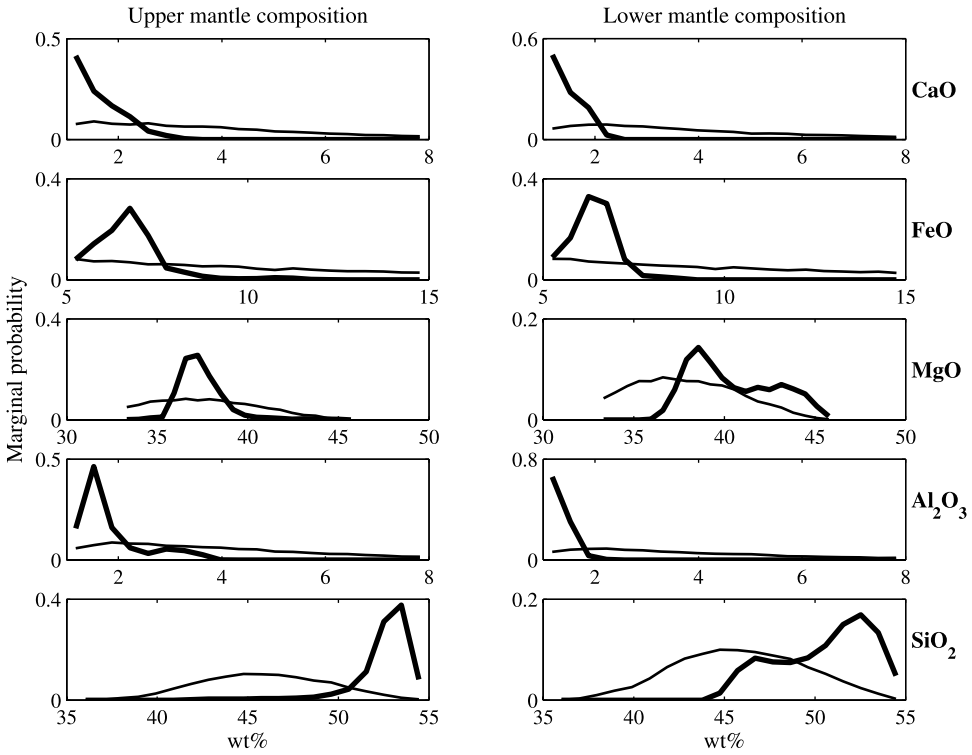

Figure 6. Prior (thin line) and posterior (thick line) marginal PDFs for the oxides in the CFMAS system (marked to the right of each panel) making up the (left) upper and (right) lower mantle composition.

[*Ringwood*, 1979; *Jagoutz et al.*, 1979; *Palme and Nickel*, 1986]. The mineralogies recovered in the inversion (Figure 10) are characteristic of those anticipated by the pyrolite model of *Ringwood* [1966].

7.3. Physical Properties I: Conductivity and Density

[46] Sampled conductivity profiles (Figure 11) compare well to the conductivity model (model III) of *Olsen* [1999]. It is reassuring that our models generally agree with the

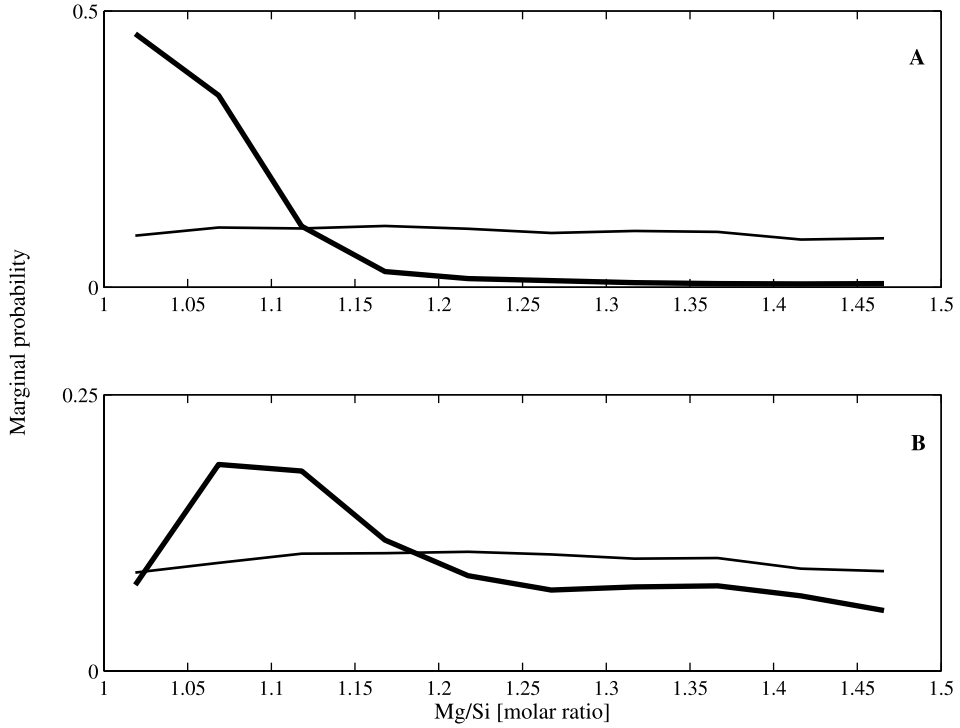

Figure 7. Prior (thin line) and posterior (thick line) marginal PDFs for calculated Mg/Si molar ratios in (a) upper mantle and (b) lower mantle using the results shown in Figure 6.

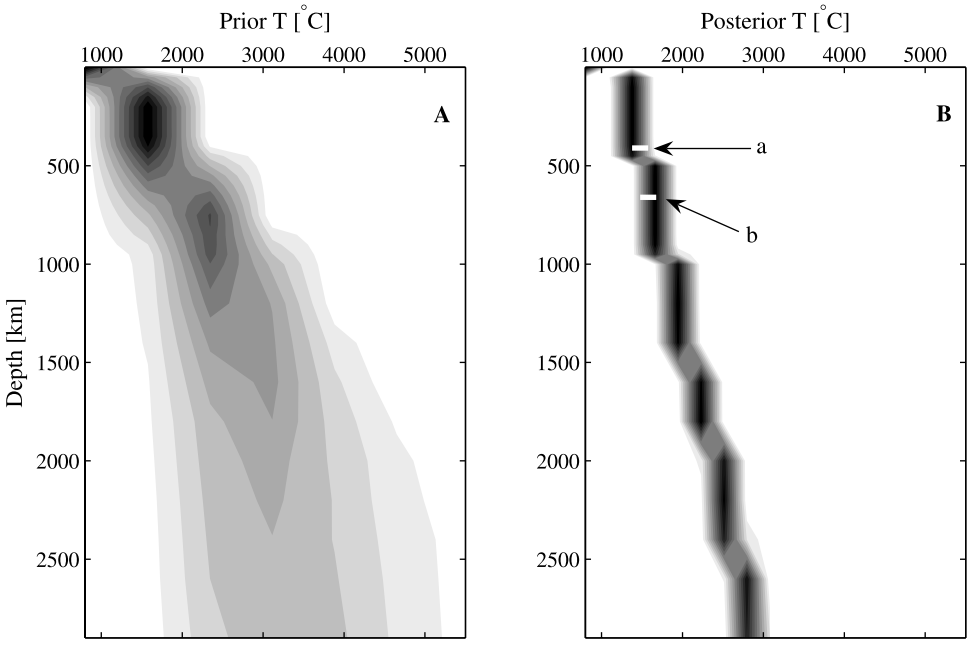

Figure 8. Marginal (left) prior and (right) posterior PDFs depicting sampled temperature models as a function of depth. At 31 fixed depth nodes a histogram reflecting the marginal probability distribution of sampled temperatures has been set up. By lining up these marginals, temperature as a function of depth can be envisioned as contours directly relating its probability of occurrence. Shades of gray between white and black indicating least and most probable outcomes, respectively. As is the case for the other parameters just shown, the posterior distribution is seen to be significantly narrowed. Experimentally determined temperatures for the reactions (a) olivine → β-spinel and (b) β-spinel → Mw + Pv, have also been included for comparison (see main text for further discussion). The width of the bars indicates experimentally determined uncertainties.

geophysically derived model of Olsen, signifying that present-day laboratory conductivity measurements have attained a quality enabling us to use these to obtain meaningful results. Two major conductivity increases are apparent; both in the neighborhood of the 410- and 660-km seismic discontinuities, the former coinciding with the appearance of the higher conducting phases wadsleyite and ringwoodite, while the latter arises because of the apparition of Mw and Pv. Of additional interest here is the excellent agreement between our sampled density models (Figure 12a) and the seismologically determined radial PREM and AK135 density profiles [*Dziewonski and Anderson*, 1981; *Kennett et al.*, 1995].

7.4. Physical Properties II: *P* and *S* Wave Velocity

[47] To further demonstrate the consistency of our results, we also calculated seismic *P* and *S* wave velocities, which

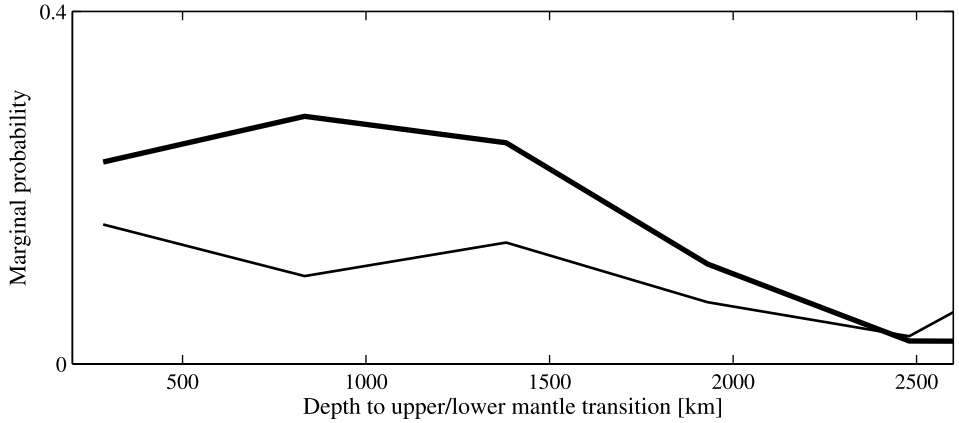

Figure 9. Prior (thin line) and posterior (thick line) PDFs, depicting sampled upper/lower mantle transition depths.

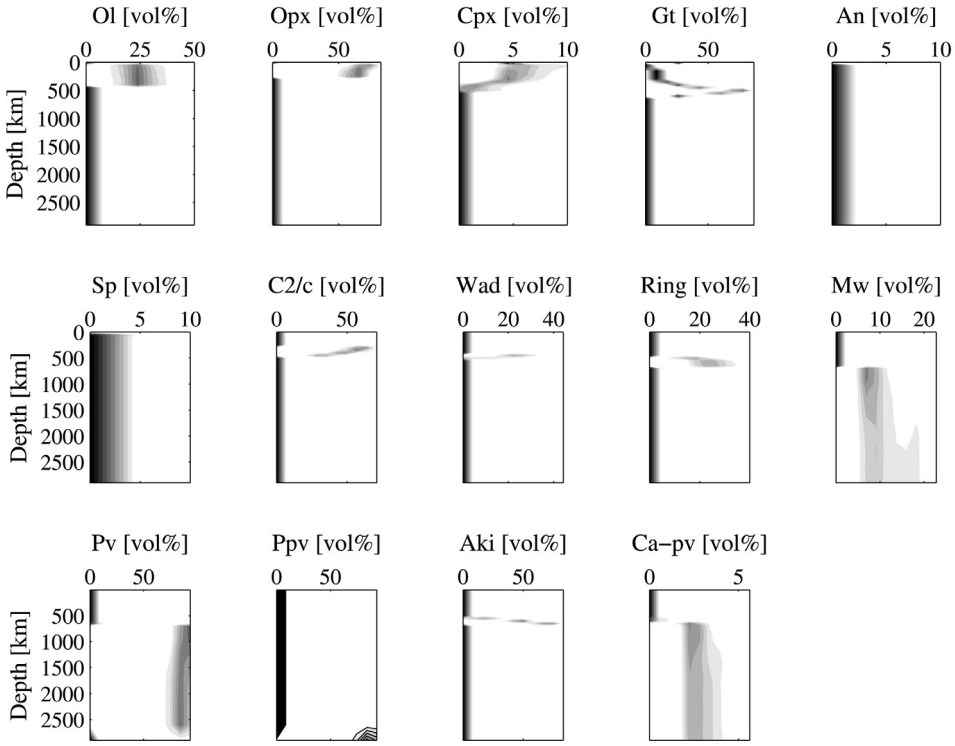

Figure 10. Marginal posterior PDFs of major minerals, showing the vol % of each phase as a function of depth. The marginals have been constructed in the same manner as in Figure 8. The mineral proportions as a function of depth can be envisioned as contours directly relating their probability of occurrence. Shades of gray as in Figure 8.

compare well with the radial v_P and v_S PREM and AK135 profiles (Figures 12b and 12c).

7.5. Convergence, Stationarity, and Resolution

[48] Convergence and resolution are important considerations for assessing the validity of inverse calculations. Convergence criteria typically include the necessity of stabilization of inverted parameter values and similarity of these across independent chains, i.e., runs, which usually provide adequate confidence in the results. Figure 13 shows the sampled temperatures at 450 km depth, obtained from the inversion of three independent posterior chains using different random number sequences. While the results vary in detail, the overall characteristics are, as expected, similar.

[49] To address the issue of data resolution, it is practical to investigate how well-resolved a certain parameter is when inverting individual data sets. Figure 13 summarizes these results, in the form of sampled temperatures at 450 km depth, for separate inversions of (1) prior information, (2) only gravity data, (3) only electromagnetic transfer functions, (4) joint inversion of all data, and (5) joint inversion of all data using different random number sequences. Inversion of individual data sets shows that while the characteristics differ among the posterior PDFs, a significant narrowing of the prior PDF is observed, signaling that individual data sets are indeed sensitive to the inverted parameter. Moreover, the posterior PDF obtained by joint inversion of all data is seen to be significantly constrained when compared to those obtained by inversion of single data sets.

8. Discussion and Conclusion

[50] It has been the purpose here to present a method of inverting electromagnetic sounding data to directly constrain composition and thermal state of the Earth. A number of considerations motivate this approach.

[51] 1. Inversions based on electrical conductivity are particularly intriguing, when compared to inversions based on seismic properties, because variations in conductivity with mineralogy are much stronger than the corresponding variations in elastic properties. In principle, electrical conductivity therefore offers a more sensitive means of probing planetary composition.

[52] 2. The approach allows the integration of a priori unrelated geophysical data sets into a joint inversion through the use of a set of model parameters that are common to all considered data sets and which describe the media studied at a fundamental level.

[53] 3. Geophysical investigations, here embodied by electromagnetic sounding analyses, are not an end in themselves in the sense that they can only be used as an indirect means to infer internal state and composition of a planet by, for example, comparing laboratory measurements of electrical conductivity made on mineral analogues with those obtained from the inversions. As such, the present approach of confronting geophysical data with

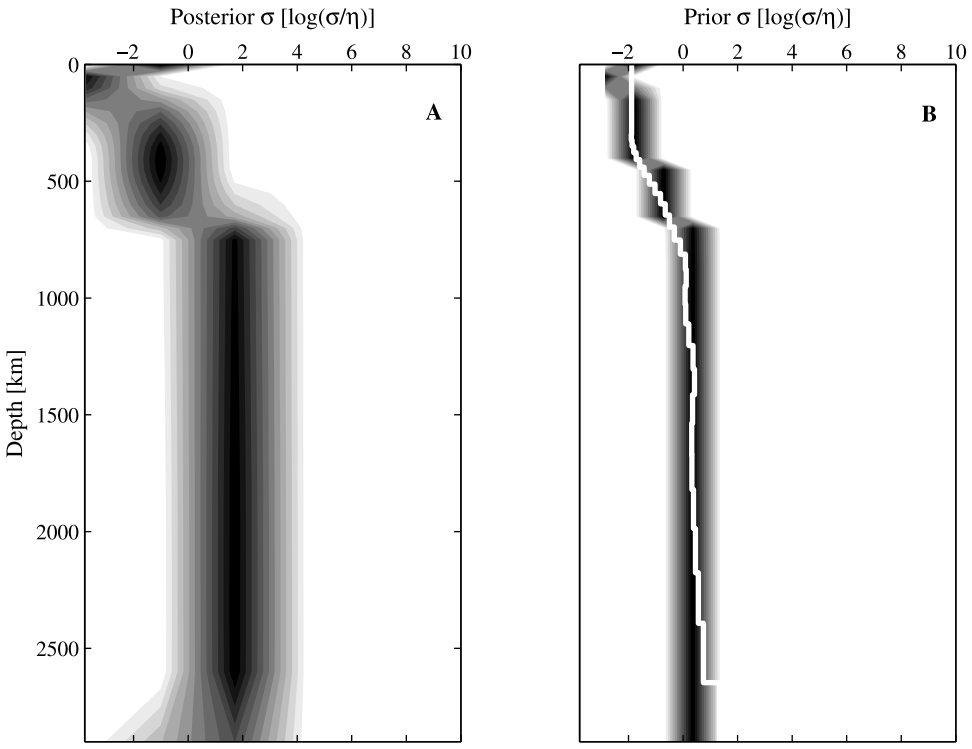

Figure 11. Marginal (a) prior and (b) posterior PDFs depicting sampled bulk conductivity profiles as a function of depth. For a comparison we included model III of *Olsen* [1999], obtained from a purely geophysical inversion of the data considered here (η = 1 S/m and shades of gray as hitherto).

compositional parameters is a step beyond the traditional geophysical sequence of first performing field measurements followed by interpretations based on laboratory results.

[54] Because we employ geophysical measurements obtained over the European continent, the results strictly apply only to the subcontinental mantle and as such do not represent true global profiles. Had we used measurements acquired over an ocean, such as those by *Utada et al.* [2003] [see also *Kuvshinov et al.*, 2005] for the North Pacific region, having a generally higher conductivity than over continents, we would probably have obtained somewhat

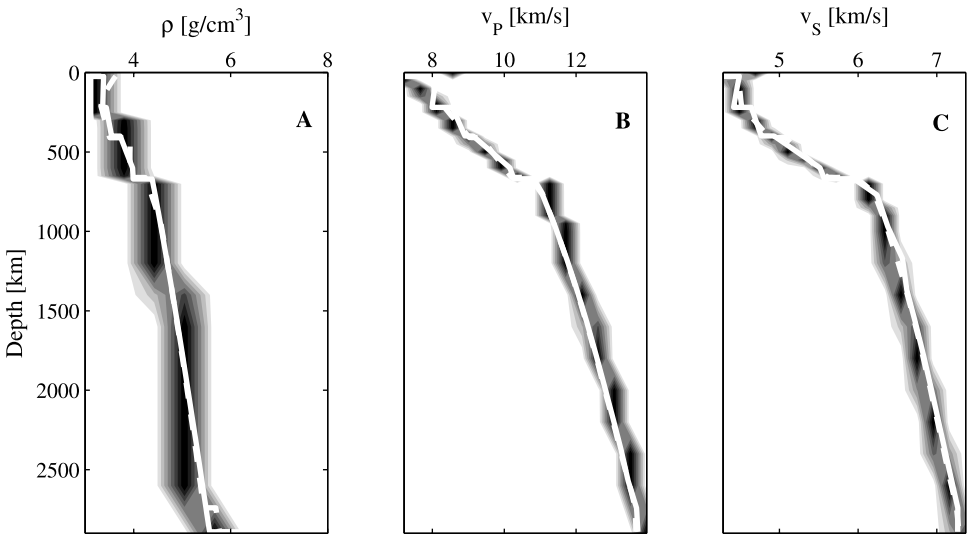

Figure 12. Marginal posterior PDFs depicting mantle physical properties as a function of depth for all sampled models of (a) density, (b) *P* wave velocity, and (c) *S* wave velocity structure. Superimposed models are PREM (solid line) and AK135 (dashed line), determined from inversion of seismic data.

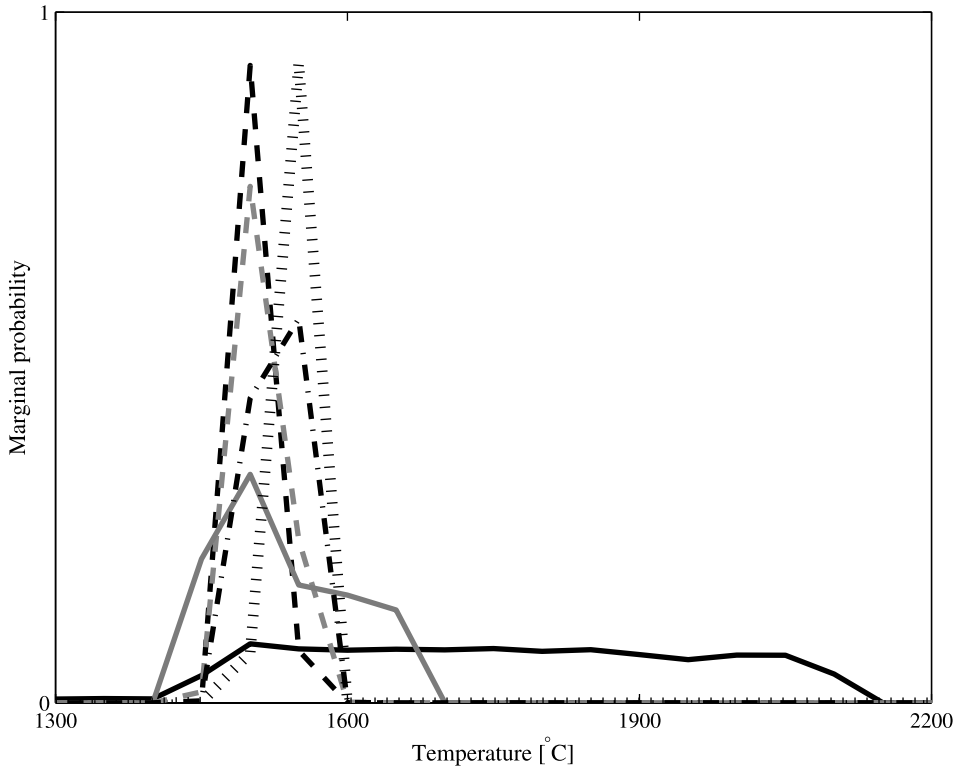

Figure 13. Marginal prior and several posterior PDFs showing sampled temperatures at a depth of 450 km, obtained from inversion of prior information (solid black line), only gravity data (solid gray line), only electromagnetic transfer function data (heavy gray dashed line), all data jointly (black dashed line), all data jointly with different random seeds (black dotted and dot-dashed line), respectively.

higher mantle temperatures. Our derived mantle geotherms are thus more likely to be representative of a lower-temperature Earth. Future application of the present method to the data set by Utada et al. will test this expectation.

[55] Given the uncertainties associated with applying experimental results to predicting mantle electrical conductivity profiles, the synthesis presented here is to be viewed as a first-order model. Our purpose was to construct such a model and to establish whether such an inversion is at all possible and if so, whether results are consistent with seismic data. The results presented can be interpreted as not only confirming the feasibility of the present approach, but also consistency with recent geophysically derived conductivity models as well as seismologically determined models, which opens the avenue for joint inversions of seismic, electromagnetic and gravity data in the future.

[56] The present approach is strongly dependent upon available laboratory electrical conductivity data, and we follow *Dobson and Brodholt* [2000a] in emphasizing that in order to carefully characterize the contributions made by individual phases to the bulk electrical conductivity profile, well-constrained laboratory measurements of those relevant phases are necessary. It is hoped that future laboratory measurements will consider more minerals, and also melts and mineral aggregates [*Roberts and Tyburczy*, 1999; *Huang et al.*, 2005], at mantle pressure-temperature conditions. An understanding of other systematics, most notably the dependence of conductivity on oxygen fugacity [*Du Frane et al.*, 2005], is also essential in order to realistically model the complexity encountered inside the Earth and other planets.

[57] **Acknowledgments.** We would like to thank A. Tarantola, an anonymous reviewer, and A. Revil for comments which improved the manuscript. Discussions with T. Shankland were also highly appreciated as were comments early on by A. Duba and Y. Xu. A. Khan gratefully acknowledges support from the Carlsberg foundation. This work was supported by Swiss National Science Funds grant 200020-101965.

References

Akaogi, M., M. Yano, Y. Tejima, M. Iijima, and H. Kojitani (2004), High-pressure transitions of diopside and wollastonite: Phase equilibria and thermochemistry of $CaMgSi_2O_6$, $CaSiO_3$ and $CaSi_2O_5$-$CaTiSiO_5$ system, *Phys. Earth Planet. Inter.*, *143*, 145.

Banks, R. J. (1969), Geomagnetic variations and the electrical conductivity of the upper mantle, *Geophys. J. R. Astron. Soc.*, *17*, 457.

Berryman, J. G. (1995), Mixture theories for rock properties, in *Rock Physics and Phase Relations: Handbook of Physical Constants*, *AGU Ref. Shelf*, vol. 3, edited by T. J. Ahrens, p. 205, AGU, Washington, D. C.

Bosch, M. (1999), Lithologic tomography: From plural geophysical data to lithology estimation, *J. Geophys. Res.*, *104*, 749.

Brown, J. M., and T. J. Shankland (1981), Thermodynamic parameters in the Earth as determined from seismic profiles, *Geophys. J. R. Astron. Soc.*, *66*, 579.

Connolly, J. A. D. (2005), Computation of phase equilibria by linear programming: A tool for geodynamic modeling and an application to subduction zone decarbonation, *Earth Planet. Sci. Lett.*, *236*, 524.

Constable, S. C. (1993), Constraints on mantle electrical conductivity from field and laboratory measurements, *J. Geomagn. Geoelectr.*, *45*, 707.

da Silva, C. R. S., R. M. Wentzcovitch, A. Patel, G. D. Price, and S. I. Karato (2000), The composition and geotherm of the lower mantle: Constraints from the elasticity of silicate perovskite, *Phys. Earth. Planet. Inter.*, *118*, 103.

Dobson, D. P. (2003), Oxygen ionic conduction in $MgSiO_3$ perovskite, *Phys. Earth Planet. Sci.*, *139*, 55.
Dobson, D. P., and J. P. Brodholt (2000a), The electrical conductivity of the lower mantle phase magnesiowüstite at high temperatures and pressures, *J. Geophys. Res.*, *105*, 531.
Dobson, D. P., and J. P. Brodholt (2000b), The electrical conductivity and thermal profile of the Earth's mid-mantle, *Geophys. Res. Lett.*, *27*, 2325.
Duba, A. (1976), Are laboratory electrical conductivity data relevant to the Earth?, *Acta Geodaet. Geophys. Montanist. Acad. Sci. Hung.*, *11*, 485.
Duba, A. G., and S. Constable (1993), The electrical conductivity of lherzolite, *J. Geophys. Res.*, *98*, 11,885.
Duba, A., H. C. Heard, and R. N. Schock (1976), Electrical conductivity of orthopyroxene to 1400°C and the resulting selenotherm, *Proc. Lunar. Planet. Sci. Conf.*, *7th*, 3173.
Duba, A., M. Dennison, A. J. Irving, C. R. Thornber, and J. S. Huebner (1979), Electrical conductivity of aluminous orthopyroxene, *Lunar Planet. Sci.*, *X*, Abstract, 318.
Du Frane, W. L., J. J. Roberts, D. A. Toffelmier, and J. A. Tyburczy (2005), Anisotropy of electrical conductivity in dry olivine, *Geophys. Res. Lett.*, *32*, L24315, doi:10.1029/2005GL023879.
Dziewonski, A. M., and D. L. Anderson (1981), Preliminary reference Earth model, *Phys. Earth Planet. Inter.*, *25*, 297.
Evans, R. L., et al. (1999), Asymmetric electrical structure in the mantle beneath the East Pacific Rise at 17°S, *Science*, *286*, 752.
Fabrichnaya, O. (1998), The assessment of thermodynamic parameters for solid phases in the Fe-Mg-O and Fe-Mg-Si-O systems, *CALPHAD Comput. Coupl. Phase Diagrams Thermochem.*, *22*, 85.
Garland, G. D. (1981), The significance of terrestrial electrical conductivity variations, *Annu. Rev. Earth Planet. Sci.*, *9*, 147.
Goddat, A., J. Peyronneau, and J. P. Poirier (1999), Dependence on pressure of conduction by hopping of small polarons in minerals of the Earth's lower mantle, *Phys. Chem. Miner.*, *27*, 81.
Guéguen, Y., and V. Palciuskas (1994), *Introduction to the Physics of Rocks*, Princeton Univ. Press, Princeton, N. J.
Hashin, Z., and S. Shtrikman (1962), A variational approach to the theory of the effective magnetic permeability of multiphase materials, *J. Appl. Phys.*, *33*, 3125.
Hastings, W. K. (1970), Monte Carlo sampling methods using Markov chains and their applications, *Biometrika*, *57*, 97.
Huang, X., Y. Xu, and S. Karato (2005), Water content in the transition zone from eletrical conductivity of wadsleyite and ringwoodite, *Nature*, *434*, 746.
Huebner, J. S., L. B. Wiggins, and A. Duba (1979), Electrical conductivity of pyroxene which contains trivalent cations: Laboratory measurements and the lunar temperature profile, *J. Geophys. Res.*, *84*, 4652.
Irifune, T. (1994), Absence of an aluminous phase in the upper part of the Earth's lower mantle, *Nature*, *370*, 131.
Ito, E., and E. Takahashi (1989), Postspinel transformations in the system Mg_2SiO_4-Fe_2SiO_4 and some geophysical implications, *J. Geophys. Res.*, *94*, 10,637.
Jagoutz, E., H. Palme, H. Baddenhausen, K. Blum, M. Cendales, G. Dreibus, B. Spettel, H. Waenke, and V. Lorentz (1979), The abundances of major, minor and trace elements in the Earth's mantle as derived from primitive ultramafic nodules, *Proc. Lunar Planet. Sci. Conf.*, *10*, 2031.
Karki, B. B., and J. Crain (1998), First-principles determination of elastic properties of CaSi (1998)O_3 perovskite at lower mantle pressures, *Geophys. Res. Lett.*, *25*, 2741.
Katsura, T., K. Sato, and E. Ito (1998), Electrical conductivity of silicate perovskite at lower-mantle conditions, *Nature*, *395*, 493.
Kennett, B. L. N., E. R. Engdahl, and R. Buland (1995), Constraints on seismic velocities in the Earth from travel times, *Geophys. J. Int.*, *122*, 108.
Keys, R. W. (1958), Volumes of activation for diffusion in solids, *J. Chem. Phys.*, *29*, 467.
Khan, A., J. A. D. Connolly, J. Maclennan, and K. Mosegaard (2006), Joint inversion of seismic and gravity data for lunar composition and thermal state, *Geophys. J. Int.*, in press.
Kuvshinov, A., H. Utada, D. Avdeev, and T. Koyama (2005), 3-D modeling and analysis of *Dst* C-responses in the North Pacific Ocean region, revisited, *Geophys. J. Int.*, *160*, 505.
Landauer, R. (1952), The electrical resistance of binary metallic mixtures, *J. Appl. Phys.*, *23*, 779.
Ledo, J., and A. G. Jones (2005), Upper mantle temperature determined from combining mineral composition, electrical conductivity laboratory studies and magnetotelluric field observations: Application to the intermontane belt, Northern Canadian Cordillera, *Earth Planet Sci. Lett.*, *236*, 258, doi:10.1016/j.epsl.2005.01.044.
Metropolis, N., A. W. Rosenbluth, M. N. Rosenbluth, A. H. Teller, and E. Teller (1953), Equation of state calculations by fast computing machines, *J. Chem. Phys.*, *21*, 1087.
Mosegaard, K. (1998), Resolution analysis of general inverse problems through inverse Monte Carlo sampling, *Inverse Problems*, *14*, 405.
Mosegaard, K., and A. Tarantola (1995), Monte Carlo sampling of solutions to inverse problems, *J. Geophys. Res.*, *100*, 12,431.
Oganov, A. R., and S. Ono (2004), Theoretical and experimental evidence for a post-perovskite phase of $MgSiO_3$ in Earth's D″ layer, *Nature*, *430*, 445.
Olsen, N. (1998), The electrical conductivity of the mantle beneath Europe derived from C-responses from 3 to 720 hr, *Geophys. J. Int.*, *133*, 298.
Olsen, N. (1999), Long-period (30 days-1 year) electromagnetic sounding and the electrical conductivity of the lower mantle beneath Europe, *Geophys. J. Int.*, *138*, 179.
Ono, S., and A. R. Oganov (2006), In situ observations of phase transition between perovskite and $CaIrO_3$-type phase in $MgSiO_3$ and pyrolitic mantle composition, *Earth Planet. Sci. Lett.*, in press.
Palme, H., and K. G. Nickel (1986), Ca/Al ratio and composition of the Earth's primitive upper mantle, *Geochim. Cosmochim. Acta*, *49*, 2123.
Parker, R. J. (1980), The inverse problem of electromagnetic induction: Existence and construction of solutions based on incomplete data, *J. Geophys. Res.*, *85*, 4421.
Parkinson, W. D. (1983), *Introduction to Geomagnetism*, Scott. Acad., London.
Parkhamenko, E. I. (1982), Electrical resistivity of minerals and rocks at high temperature and pressure, *Rev. Geophys.*, *20*, 193.
Phillips, R. J. (1972), The Lunar conductivity profile and the nonuniqueness of electromagnetic data inversion, *Icarus*, *17*, 88.
Ringwood, A. E. (1966), Mineralogy of the mantle, in *Advances in Earth Science*, edited by P. Hurley, p. 357, MIT Press, Cambridge, Mass.
Ringwood, A. E. (1975), *Composition and Petrology of the Earth's Mantle*, McGraw-Hill, New York.
Ringwood, A. E. (1979), *Origin of the Earth and Moon*, Springer, New York.
Roberts, J. J., and J. A. Tyburczy (1999), Partial-melt electrical conductivity: Influence of melt composition, *J. Geophys. Res.*, *104*, 7055.
Schmucker, U. (1970), Anomalies of geomagnetic variations in the southwestern United States, *Bull. Scripps Inst. Ocean., Univ. Calif.*, *13*, 1.
Schock, R. N., A. G. Duba, and T. J. Shankland (1989), Electrical conduction in olivine, *J. Geophys. Res.*, *94*, 5829.
Schubert, G., D. L. Turcotte, and P. Olson (2001), *Mantle Convection in the Earth and Planets*, Cambridge Univ. Press, New York.
Schulgasser, K. (1976), Relationship between single-crystal and polycrystal electrical conductivity, *J. Appl. Phys.*, *47*, 1880.
Shankland, T. J. (1975), Electrical conduction in rocks and minerals: Parameters for interpretation, *Phys. Earth Planet. Inter.*, *10*, 209.
Shankland, T. J., and A. Duba (1990), Standard electrical conductivity of isotropic, homogeneous olivine in the temperature range 1200–1500°C, *Geophys. J. Int.*, *103*, 25.
Shankland, T. J., J. Peyronneau, and J. P. Poirier (1993), Electrical conductivity of the Earth's lower mantle, *Nature*, *366*, 453.
Srivastava, S. P. (1966), Theory of the magnetotelluric method for a spherical conductor, *Geophys. J. R. Astron. Soc.*, *11*, 373.
Stacey, F. D. (1977), *Physics of the Earth*, 2nd ed., John Wiley, Hoboken, N. J.
Stacey, F. D., and O. L. Anderson (2001), Electrical and thermal conductivities of Fe-Ni-Si alloy under core conditions, *Phys. Earth Planet. Inter.*, *124*, 153.
Stixrude, L., and M. S. T. Bukowinski (1990), Fundamental thermodynamic relations and silicate melting with implications For the constitution Of D″, *J. Geophys. Res.*, *95*, 19,311.
Stixrude, L., and C. Lithgow-Bertelloni (2005a), Mineralogy and elasticity of the oceanic upper mantle: Origin of the low-velocity zone, *J. Geophys. Res.*, *110*, B03204, doi:10.1029/2004JB002965.
Stixrude, L., and C. Lithgow-Bertelloni (2005b), Thermodynamics of mantle minerals - I. Physical properties, *Geophys. J. Int.*, *162*, 610.
Tarantola, A. (2004), *Inverse Problem Theory and Model Parameter Estimation*, SIAM, Philadelphia, Penn.
Tarantola, A., and B. Valette (1982), Inverse problems: Quest for information, *J. Geophys.*, *50*, 159.
Utada, H., T. Koyama, H. Shimizu, and A. D. Chave (2003), A semi-global reference model for electrical conductivity in the mid-mantle beneath the North Pacific region, *Geophys. Res. Lett.*, *30*(4), 1194, doi:10.1029/2002GL016092.
Watt, J. P., G. F. Davies, and R. J. O'Connell (1976), The elastic properties of composite materials, *Rev. Geophys.*, *14*, 541.
White, W. B., S. M. Johnson, and G. B. Dantzig (1958), Chemical equilibrium in complex mixtures, *J. Chem. Phys.*, *28*, 751.
Wood, B. J., and J. R. Holloway (1984), A thermodynamic model for subsolidus equilibria in the system CaO-MgO-Al_2O_3-SiO_2, *Geochim. Cosmochim. Acta*, *66*, 159.

Xu, Y., and C. McCammon (2002), Evidence for ionic conductivity in lower mantle (Mg,Fe)(Si,Al)O_3 perovskite, *J. Geophys. Res.*, *107*(B10), 2251, doi:10.1029/2001JB000677.

Xu, Y., and T. J. Shankland (1999), Electrical conductivity of orthopyroxene and its high pressure phases, *Geophys. Res. Lett.*, *26*, 2645.

Xu, Y., B. T. Poe, T. J. Shankland, and D. C. Rubie (1998a), Electrical conductivity of minerals of the mantle transition zone, *Science*, *280*, 1415.

Xu, Y., C. McCammon, and B. T. Poe (1998b), The effect of alumina on the electrical conductivity of silicate perovskite, *Science*, *282*, 922.

Xu, Y., T. J. Shankland, and A. Duba (2000a), Pressure effect on electrical conductivity of mantle olivine, *Phys. Earth Planet. Inter.*, *118*, 149.

Xu, Y., T. J. Shankland, and B. T. Poe (2000b), Laboratory-based electrical conductivity in the Earth's mantle, *J. Geophys. Res.*, *108*, 2314.

Yoder, C. F. (1995), Astrometric and geodetic properties of Earth and the solar system, in *A Handbook of Physical Constants: Global Earth Physics*, *AGU Ref. Shelf*, vol. 1, edited by T. J. Ahrens, p. 1, AGU, Washington, D. C.

J. A. D. Connolly, Earth Sciences Department, Swiss Federal Institute of Technology, Soneggstr. 5, CH-8092 Zurich, Switzerland. (james.connolly@erdw.ethz.ch)

A. Khan, Niels Bohr Institute, University of Copenhagen, Juliane Maries Vej 30, DK-2100 Copenhagen Oe, Denmark. (amir@gfy.ku.dk)

N. Olsen, Danish National Space Centre, Juliane Maries Vej 30, DK-2100 Copenhagen Oe, Denmark. (nio@spacecenter.dk)